Desalination and Water Treatment
www.deswater.com

doi:10.5004/dwt.2019.24495

165 (2019) 54–62
October

Incorporation of magnetite nanoparticles in poly(vinyl chloride) microfiltration membrane for improving antifouling property and desalination performance

Majed M. Alghamdi[a,b,*], Adel A. El-Zahhar[a,b], Badriah M. Asiri[b]

[a]*Environmental Monitoring, Assessment & Treatment (EMAT) Research Group, Department of Chemistry, College of Science, King Khalid University, P.O. Box 9004, Abha 61413, Saudi Arabia, Tel. +966-535462798, email: mmalghamdi@kku.edu.sa (M.M. Alghamdi), elzahhar@kku.edu.sa (A.A. El-Zahhar)*
[b]*Department of Chemistry, Collage of Science, King Khalid University, P.O. Box 9004, Abha 61413, Saudi Arabia, email: bdra3h2@hotmail.com (B.M. Asiri)*

Received 26 February 2019; Accepted 2 June 2019

ABSTRACT

In this paper, poly(vinyl chloride) (PVC) nanocomposite membranes were fabricated with different content ratios of magnetite nanoparticles (MNPs) (0–10 wt %), using phase inversion method to improve the PVC membrane performance and its physicochemical properties. Membranes were characterized by different techniques including Fourier transform infrared, X-ray diffraction, thermal gravimetric analysis, contact angle measurements and scanning electron microscopy. X-ray diffraction studies revealed the formation of the exfoliated structure. Thermal gravimetric analysis studies suggested better thermal stability after the addition of MNPs. The experimental performance results demonstrated an enhancement of water flux, solute rejection, and antifouling properties up to a loading of 10% MNPs. In particular, the composite membrane of 6% MNPs exhibited an optimum performance of around 55% improvement in water flux. Moreover, it demonstrated an improvement of around 40% in salt rejection for NaCl, LiCl, and $MgSO_4$ and around 37% for Na_2SO_4, compared to the pure PVC membrane. Furthermore, it illustrated a flux recovery ratio of around 89%, representing the highest improvement with 22% improvement compared to the pure PVC.

Keywords: Poly(vinyl chloride) (PVC); Membrane; Magnetite nanoparticles (MNPs); Composite; Antifouling

1. Introduction

The membrane technology, due to its versatility and efficiency, has drawn considerable attention as a prospective separating process with the possibility of wide applications in the future. To achieve this purpose, a broad range of polymers have been devised. As a type of material that can be applied to membranes, PVC polymerhas not attracted equal attention, although it is a major type of commercial plastic mainly because of its broad applications and low cost. In fact, promoting properties such as low cost and devising diverse polymers such as PVC to be used in membranes can advance membrane application, even in the rural areas. The potential application of PVC membranes has been reported in a few studies in the literature. For example, the enhancement of the properties and performance of PVC membranes through the addition of polyvinyl butyral [1], PVP/PEG [2], and most recently nano-Fe_2O_3 has been reported in the literature [3]. Also,PVC copolymers membranes were reported with improved performance and antifouling properties [4–6].

Polymer-based materials, in general, are reasonably cheap, hence their widespread use in membrane fabrication. However, polymer backbones are highly hydrophobic and susceptible to extensive fouling, and thus they cannot be used without modifications [7]. Although several methods have been used to enhance the performance of polymeric-based membranes by increasing the hydrophilicity and fouling resistance [8–10], the incorporation of different types of nanoparticles into membranes has attracted considerable

*Corresponding author.

attention. In fact, the incorporation of nanoparticles into the polymeric matrix has proven to yield desirable results, and the rationale behind the great interest in nanoparticles is because of the capability of nanomaterials to produce unique characteristics that can largely improve properties such as fouling tendency, selectivity, and permeability. Although different types of nanoparticles such as titanium oxide [11–15], zinc oxide [16,17], alumina [18], silica [19,20], graphene oxide [21], and carbon nanotube [22,23] have widely been used to improve the properties of membranes, PVC has not been sufficiently studied.

Magnetite nanoparticles (MNPs), in particular, have been also considered as an additive due to their unique characteristics such as physicochemical properties and good biocompatibility. The incorporation of magnetite in membranes has been reported for several polymeric-based membranes such as PVDF [24], polysulfone [25] and polyethersulfone [26], resulting in the improvement of the antifouling properties. However, the effect of magnetite on PVC-based membranes has not been investigated. In this work, PVC composite membranes with different loading of MNPs were prepared. The objective is to study the effect of MNPs on the properties and performance of PVC composite membranes.

2. Experimental

2.1. Materials

Poly (vinyl chloride) with Mn ~ 22,000 and Mw ~ 43,000 was supplied from Aldrich. Dimethylformamide (DMF) was obtained from PROLABO. All other chemicals used in this study were analytical grade and were purchased from Sigma-Aldrich© and used as received unless otherwise stated.

2.2. Preparation of the magnetic nanoparticles

Ferrous sulfate solution was prepared by dissolving 1 g of $FeSO_4$ in 100 mL of distilled water and stirred via magnetic stirrer until complete dissolution was achieved. Sodium hydroxide solution of 1 mol/L was prepared by dissolving 4 g of NaOH in 100 mL of distilled water. Sodium hydroxide solution was added at a very slow rate (1 mL/10 min) to the ferrous sulfate solution. The pH of the reaction was measured after each 1 mL addition of NaOH solution. The addition was continued until the pH value of 12 was achieved. The obtained black suspension was completed to 200 mL with distilled water and placed in the microwave at half power for 10 min. The formed black MNPs were repeatedly washed with distilled water until neutral pH was attained. Subsequently, the prepared MNPs were separated via centrifugation and dried until a constant weight was achieved.

2.3. Membrane preparation

The composite membranes of PVC and MNPs were prepared via the phase-inversion technique. First, MNPs with varying amounts were dispersed in DMF and stirred for one hour to verify the complete dispersion of MNPs in the solvent. The obtained suspension was then sonicated for one hour to ensure that the particles were well dispersed in the solution. Second, the PVC with 17 wt% in DMF was prepared and stirred until complete dissolution was achieved. Next, the prepared MNPs suspension was added to the PVC solution with continuous stirring for 12 h until a homogenous solution was formed. The absolute compositions of the prepared casting solutions are presented in Table 1. Afterward, to remove the air bubbles, a vacuum oven was used for 12 h and before the solution was cast on a glass plate. A casting knife was then utilized to obtain the cast film (thickness of 0.6 mm), which was straight away submerged into a coagulation bath of distilled water. Subsequently, the obtained film was washed several times with distilled water to remove the residual solvent and was stored in the distilled water for further examination.

2.4. Membrane characterization

Fourier transform infrared spectroscopy (FT-IR) analysis was performed using Nicolet 6700 FTIR model from Thermo-Scientific. The samples were mixed with potassium bromide and compressed to obtain a disk. The spectra of the obtained disks were then analyzed in the IR region of 400–4000 cm^{-1}. Moreover, Shimadzu 6000DX instrument (from Shimadzu Corporation, Japan) was used to carry out the XRD analysis, using the CuKα sealed tube operated at 40 kV and 30 mA and measured from 5 to 80°2θ at 0.020 step with λ = 0.154056 nm. Furthermore, the field emission scanning electron microscopy was utilized for the evaluation of the morphology of the samples. Images were obtained using a Jeol Model 6360 LV SEM (USA). The thermal gravimetric analysis was also measured on Shimadzu TGA-50H thermal analyzers. The sample with around 15 mg in a platinum crucible was heated within a temperature range of 30–800°C and at a heating rate of 10°C min^{-1} with a controlled nitrogen flow of 40 cm^3 min^{-1}. Finally, the static water contact angle was used to evaluate the hydrophilicity and wettability of the membrane surface using distilled water.

3. Membrane properties

3.1. Pore size, porosity and water uptake

The membrane properties such as porosity, pore size and water uptake were investigated. The volume fraction method was applied to calculate the porosity and water uptake values of the prepared membrane. The following

Table 1
Composition of casting solutions for PVC-MNPs

Membrane code	PVC (wt/wt%)	MNPs (wt/wt%)
PVC	100	0
PVC-MNP 2%	98	2
PVC-MNP 6%	94	6
PVC-MNP 10%	90	10

equations were used for porosity and water uptake calculation, respectively [16,27].

$$\varepsilon = \frac{W_w - W_d}{\rho_w \left(\pi r^2 l\right)} \times 100\% \quad (1)$$

$$\text{Water uptake} = \frac{W_w - W_d}{W_d} \times 100\% \quad (2)$$

where W_w (g) denotes weight for wet membrane, and W_d (g) denotes the weight for dry membrane. l and r (cm) are the thickness and radius of the membrane, respectively. ρ_w (g/cm^3) is the density of the water at 25°C.

Moreover, the mean pore diameter of the prepared membrane was estimated according to Eq. (3) [13,22].

$$a = \sqrt{\frac{(2.9 - 1.75\varepsilon) \times 8\mu l Q_w}{\varepsilon A \Delta P}} \quad (3)$$

where a (m) is the mean pore diameter. Q_w (m^3/s) is the pure water flux. A (m^2) and l (m) are the filtration area of the membrane and the thickness of the membrane, respectively. μ (Pa·s) is the viscosity of the water at 25°C. ΔP (Pa) is the transmembrane pressure, and ε is the porosity.

3.2. Pure water flux and rejection ratio

The performance of the membrane was studied using the dead-end membrane filtration system. The performance was also evaluated at differentially applied membrane pressures (0.2–1.1 MPa). The applied membrane pressure (AMP) was manually adjusted during the runs by manual injector compression. The pure water flux (J_w) was determined according to Eq. (4).

$$J_w = \frac{V}{A \cdot t} \quad (4)$$

where V (L) denotes the permeate volume, which is collected during the time interval t (h), and A (m^2) is the effective area of the membrane.

The rejection efficiency of the membranes was studied by performing the filtration of the inorganic salt solutions of $MgSO_4$, Na_2SO_4 and NaCl individually at a constant membrane pressure of 0.2 MPa after flux stability (after at least 6 h). The feed solutions were prepared at 1 g/L and pH = 6.0. The pH was regulated by the addition of 0.1 mol/L HCl or NaOH. The feed and the collected permeate were tested using a conductivity meter. The solute rejection percentage (SR) was then attained by Eq. (5) as shown below.

$$SR\% = \left(1 - \frac{C_p}{C_f}\right) \times 100\% \quad (5)$$

where C_f and C_p are the concentrations in the feed and the permeate solutions, respectively.

3.3. Antifouling performance

Sodium alginate (SA) was used in the fouling experiments as a model of an organic foulant. The experiments were carried out using 20 mg/L SA and 10 mM NaCl solution as follows: First, the SA solution was applied as a feed solution until the flux was almost stable. Then, the flux equipment parts and membranes were washed out with distilled water. After cleaning, the experiments were repeated with distilled water. This was done to evaluate the pure water flux and to determine the flux recovery ratio (FRR) using Eq. (6).

$$FRR\% = \left(\frac{J_{w2}}{J_{w1}}\right) \times 100\% \quad (6)$$

where J_{w1} is the pure water flux before fouling experiment and J_{w2} is the pure water flux after the fouling experiment.

4. Results and discussion

4.1. Fourier transform infrared (FT-IR) analysis

Fig. 1 shows the FT-IR spectra of MNPs, PVC, and the composites. The peak at around 579 cm^{-1}was attributed to the Fe-O characteristic stretching vibration. In comparison, the infrared spectra, obtained for the composite spectra, showed PVC polymer characteristic peaks of around 2970 and 2910 cm^{-1} for C-H stretching, 1427cm^{-1} for CH_2 bending, 1099 cm^{-1} for C-C stretching, and 616 cm^{-1} for C-Cl stretching. Besides the characteristic peaks of PVC, as a result of the addition of MNPs, bands at 3440cm^{-1} and 1676 cm^{-1} appeared in the composites spectra and corresponded to O-H stretching and bending, respectively.

4.2. XRD analysis study

The XRD pattern of MNPs and the composite membranes are shown in Fig. 2. The XRD pattern for MNPs exhibited the characteristic pattern of MNPs (Fe_3O_4). The peaks appeared at 2θ of 30.21°, 35.57°, 37.20°, 43.23°, 53.63°, 57.17°, and 62.77°, corresponding to pure Fe_3O_4, and were consistent with the standard data JCPDS 65-3107. Moreover, MNPs showed a dominant peak at 2θ = 35.57°, corresponding to a d-spacing of 2.52 A°. The approximated crystallite size, associated with the peak at 35.57°, was of around 27

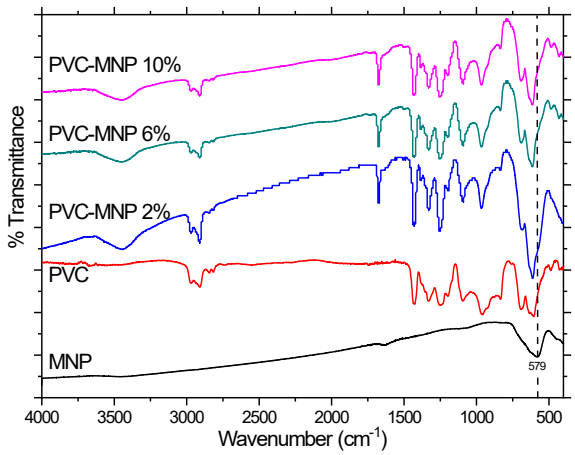

Fig. 1. FT-IR spectra of MNPs, PVC and PVC-MNPs composite membranes.

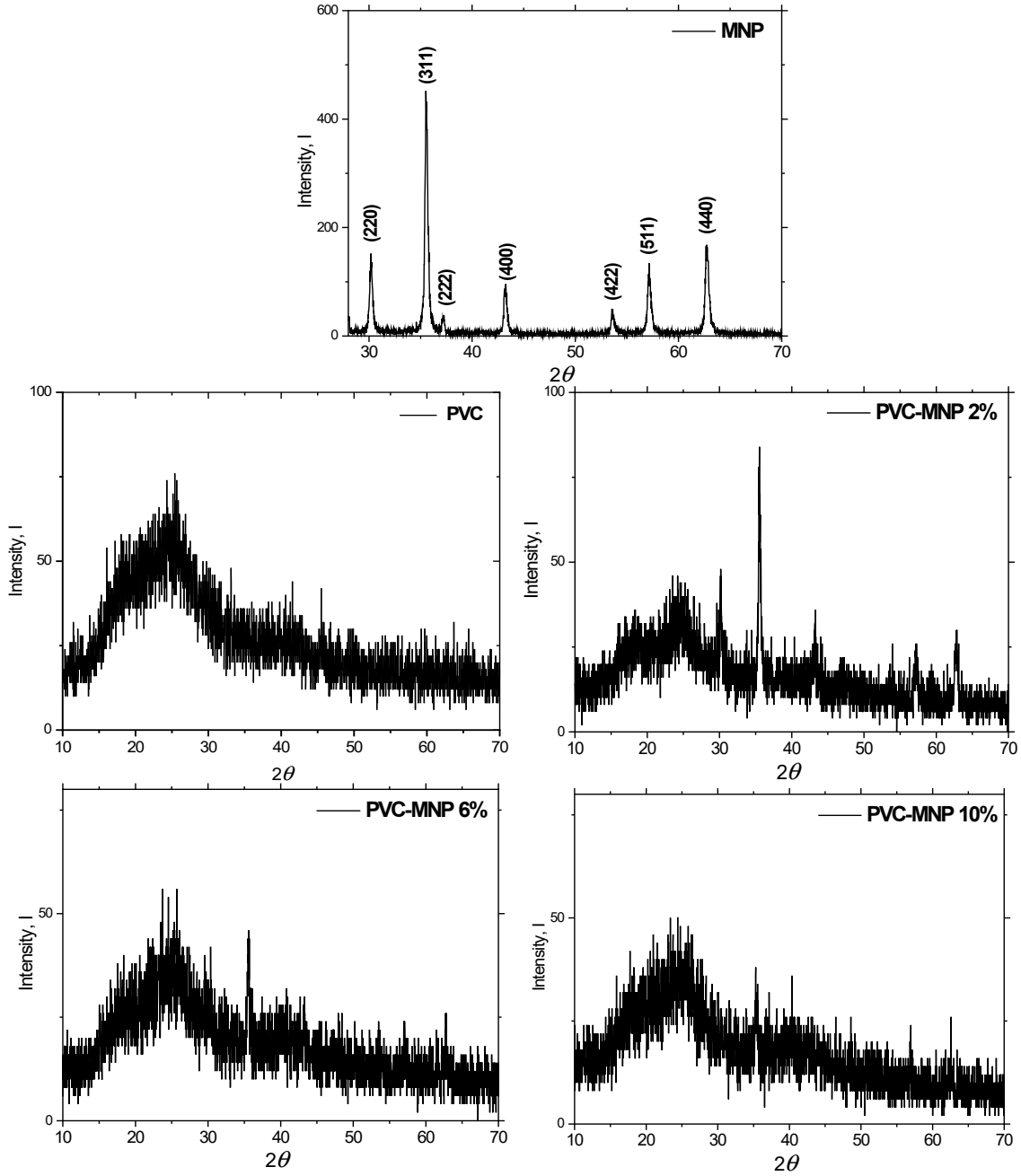

Fig. 2. XRD of MNPs, PVC, and the composite membranes.

nm, which was calculated using Scherrer's equation [28] and determined using the following formula:

$$D_c = \frac{K\lambda}{\beta \cos\theta} \tag{7}$$

where D_c is the crystallite size in nm, K is the so-called shape factor = 0.89, λ = 0.154056 nm, β is the full width at half maximum (FWHM), and θ is the diffraction angle.

In contrast, XRD of the composites revealed an amorphous morphology. The original characteristic peaks of MNPs decreased and slightly shifted or disappeared in the composite diffractograms with the addition of MNPs. These findings confirm the formation of the exfoliated composite.

4.3. Morphology of the membranes

The morphology of the polymer composite membranes was studied using the scanning electron microscopy (SEM) analysis (see Fig. 3 for the results). Differences were observed between the PVC surfaces that had been taken before and after the addition of MNPs. The addition of MNPs had a noticeable effect on the surface morphology. The pure PVC

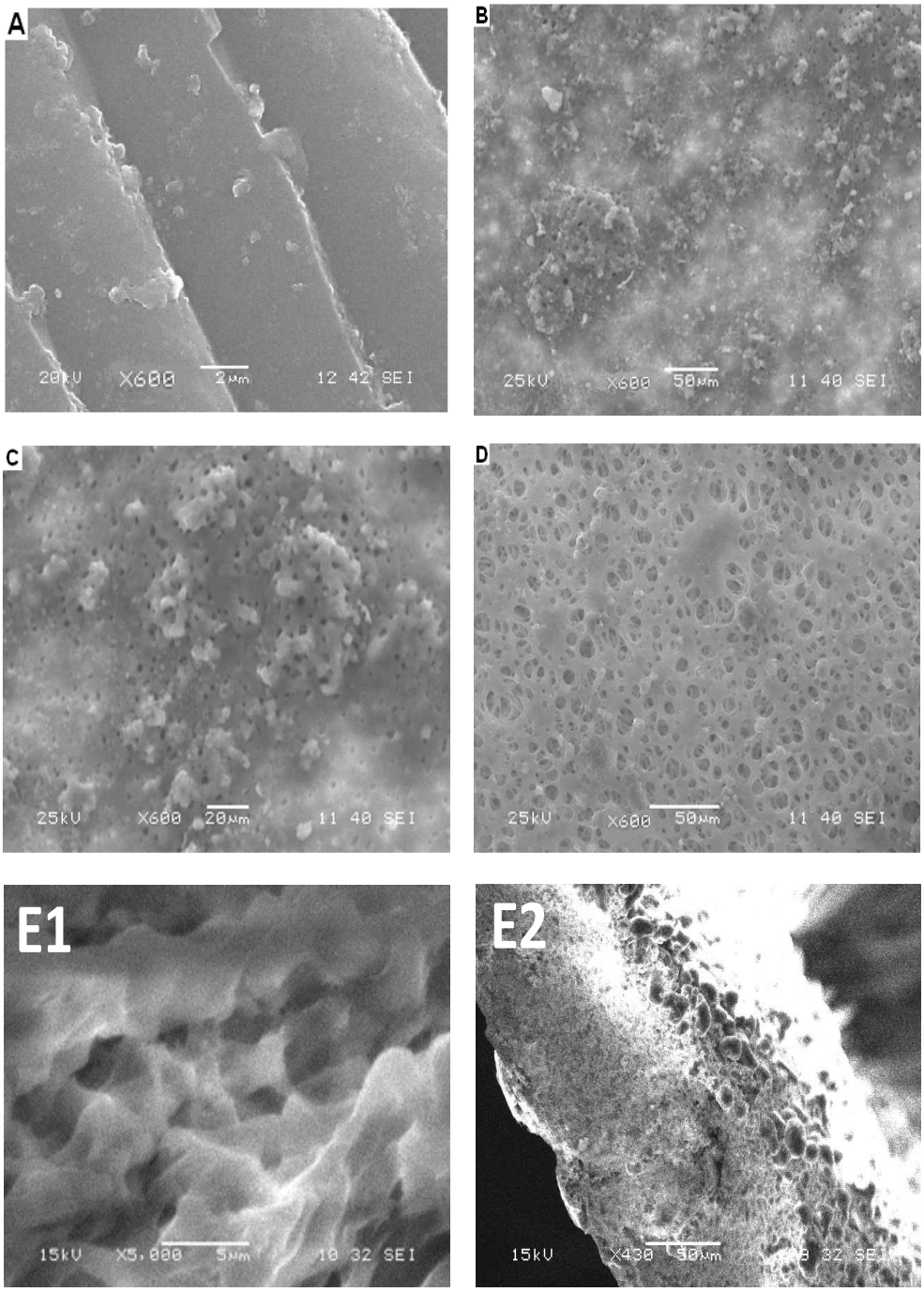

Fig. 3. SEM images of PVC and PVC-MNP composite membranes: A) pure PVC, B) PVC-MNP 2%, C) PVC-MNP 6%, D) PVC-MNP 10%, E1) cross-sectional for PVC, E2) cross-sectional for PVC-MNP 6%.

had a smoother surface, and surface roughness increased with the addition of MNPs, as evident in the SEM images. Furthermore, the smoothness of the surface was found to decrease with the addition of MNPs. As Fig. 3 illustrates, the composite membranes exhibited porous surfaces compared to the pure PVC. It is clear that increasing the content of MNPs by 10% resulted in greater pores compared to the other composite membranes. This observed porous structure could be explained by the great solvent-water exchange rate through the phase-inversion preparation process [29]. Moreover, it is known that increasing the content of MNPs in the solution will increase the viscosity of the solution and affect the water solvent exchange through the phase-inversion process, which may, in turn, alter the surface structure and affect the size of the pores. This also may cause the formation of macrovoids, resulting in greater pore size, supported by the trend obtained after increasing the MNPs by 10%. In addition to the above mentioned results, Fig. 3E also displays the differences in the cross-sectional images of the pure PVC and PVC-MNP 6% membrane.

4.4. Properties of the membranes

The effects of the content of MNPs on the porosity and the mean pore size diameter are listed in Table 2. The results showed that both porosity and the mean pore size increased after the addition of MNPs, which had the largest value with the content of 2% of MNPs. This increase could be related to the adsorption and the hydrophilic properties of the MNPs, which could improve the exchange between solvent and water during the phase inversion, and hence increases the pore size and the interconnectivity within the membrane layers, which, in turn, controls the permeability [30,31].

4.5. Contact angle measurements

Fig. 4A illustrates that the contact angle of pure PVC membrane is 77°, which is consistent with the literature [1]. The addition of MNPs resulted in variations in hydrophilicity. The membrane with a 6% addition of MNPs exhibited a more hydrophilic character. This might be due to the hydrophilic nature of the MNPs. However, with the addition of 10% of MNPs, the membrane exhibited a lower hydrophilic character. However, the water uptake of the composite membrane improved by up to 121%, as compared to the pure PVC (see Fig. 4B). This water uptake improvement can be an indication of the hydrophilic sub-surface bulk of the PVC-MNPs membranes, arising from the incorporation of MNPs into the polymer structure. This is consistent with what has been reported in literature for PVDF/MNPs membrane, where the addition of MNPs also resulted in more hydrophobic character [24].

Table 2
Properties of the PVC-MNP % composite membranes

Fe_3O_4 content (wt%)	Porosity %	Thickness (mm)	Mean pore diameter (nm)
0	81	0.3	21
2	94	0.3	52
6	91	0.3	50
10	90	0.3	50

4.6. Thermal gravimetric analysis

Based on the observation of a mass loss data at all temperature intervals in TGA curves, different degradation peaks were recorded. One degradation peak was observed for the pure PVC, whereas three degradation peaks were observed for the 2% and 6% MNPs composites, and two peaks for the 10% MNPs composite (Fig. 5). For the pure PVC, an interval between 221–734°C was observed. For the composite membranes, the last step was predominantly the weight loss characteristic degradation step of the polymer structure. For the 2%, 6%, and 10% MNPs composite membranes, the degradation was observed between 426–786°C, 396–528°C and 419–636°C, respectively. If we consider the decomposition temperature at the characteristic degradation step, the results clearly indicate higher thermal decomposition temperatures and lower weight loss for the composite membranes. Accordingly, the MNPs-loaded membranes demonstrated better thermal stability than the pristine PVC.

4.7. Membrane performance

The experimental results for membranes performance included the pure water flux, solute rejection and antifouling of the differentially prepared nanocomposite membranes. As Fig. 6A shows, the pure water flux increased with pressure as well as the presence of MNPs until it reached a maximum of around 1310 L/m² h at 10% MNPs composite membrane at 1.1 MPa pressure. This development can be attributed to the increase in the permeability of the composite membrane, as shown in Table 2 and the SEM images. The increase in the permeability was due to the rise in the porosity and the mean pore size after the addition of MNPs. i.e. more content ratio of MNPs could change the casting solution properties and consequently change the surface structure and surface properties.

Fig. 6A also shows the effect of the applied pressure on the pure water flux measurements, indicating the stability of the membrane. The water fluxes of all the membranes were almost linear, with a pressure change up to around 0.6 MPa, exhibiting resistance to deformation. Next, the flux values

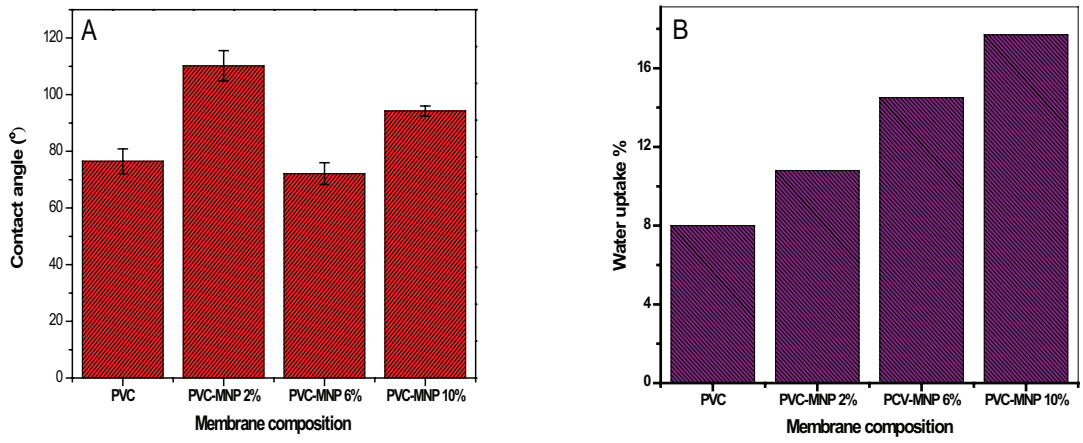

Fig. 4. A) Static water contact angle of PVC and composite membranes with different MNPs concentrations. B) Water uptake values of PVC-MNP % composite membrane.

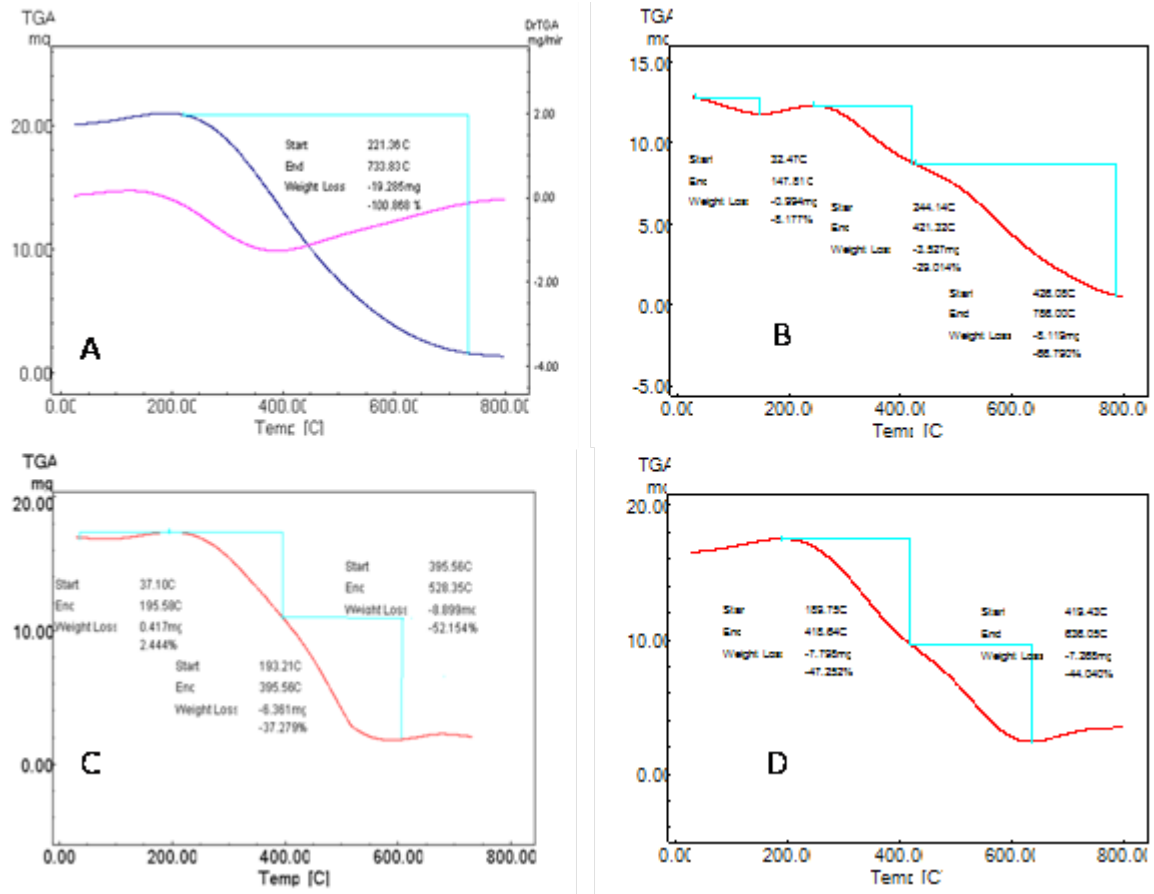

Fig. 5. TGA curves of A) pure PVC, B) PVC-MNP 2%, C) PVC-MNP 6%, D) PVC-MNP 10% composite membranes.

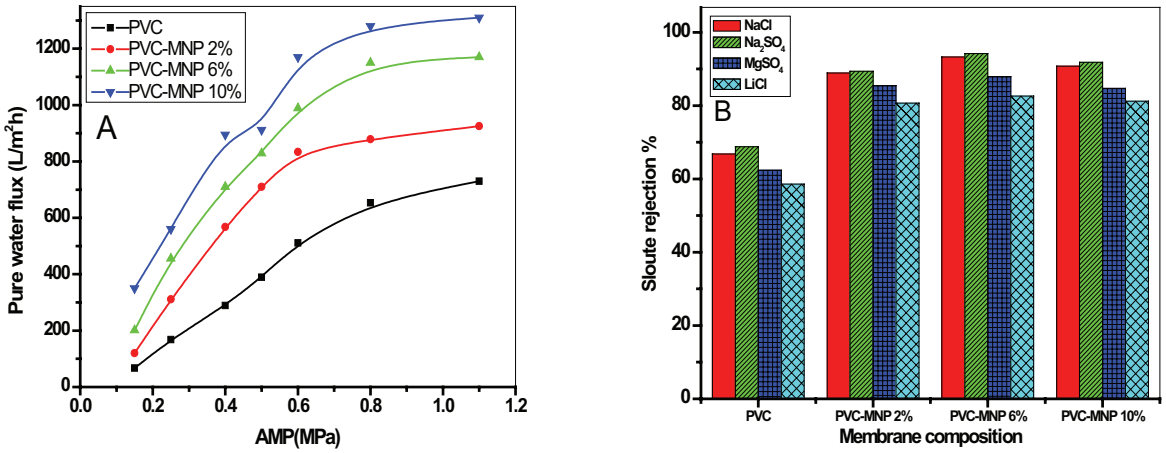

Fig. 6. A) Variation of water flux under differentially applied transmembrane pressure and MNPs-loading concentrations. B) Solute rejection of PVC-MNP % composite membranes, performed at constant pressure of 0.2 MPa.

started to become somewhat steady due to pore deformation. However, the composite membranes appeared to be more susceptible to compaction with pressure above 0.6 MPa, particularly for the 2% and 10% MNPs-loaded membranes compared to the pure PVC.

Moreover, as Fig. 6B illustrates, all the studied composite membranes exhibited considerable rejection level from around 81% to 94 %, varying with solute types. Obviously,this study revealed up to 40% enhancement of the solute removal after the addition of MNPs. Similar solute rejection

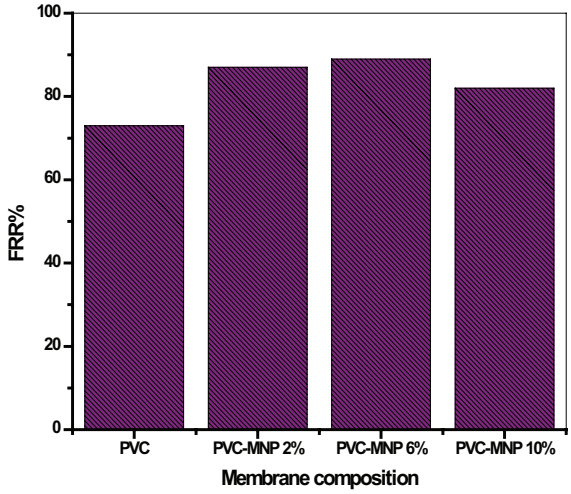

Fig. 7. Water flux recovery ratio of PVC-MNP% membranes after SA fouling.

patterns were observed in the following sequence: Na_2SO_4 > NaCl > $MgSO_4$ > LiCl. For example, with the PVC-MNP 6% composite membrane, the rejection ratio obtained for NaCl and Na_2SO_4 were 93% and 94%, respectively. In contrast, $MgSO_4$ and LiCl showed lower ratios of around 88% and 83%, respectively. These results revealed the enhancement of the solutes removal despite the observed increase in the pore diameter after the addition of MNPs (Table 2), which suggested the possible influence of the other factors. In fact, the obtained enhancement could be attributed to the influence of factors such as surface charges, membrane morphology, and MNPs high adsorption efficiency for ions. Certainly, the obtained results demonstrate an enhanced membrane performance for both permeability and solute rejection, breaking the known trade-off relationship between permeability and selectivity. Furthermore, besides the water treatment potential applications of the prepared composite membranes, the obtained results also indicate the potential applicability of the composite membrane for water softening.

To study the antifouling properties of the membranes and the effect of the additive content on fouling, the FRR analysis was performed for the prepared membranes. According to Fig. 7, the pure PVC membrane showed a FRR value of around 73%. The addition of MNPs led to an apparent enhancement in antifouling properties, resulting in higher FRR values. In particular, PVC-MMT 6% composite membrane showed the highest FRR of around 89%, representing around 22% enhancement compared to the pure PVC. The improvement of the FRR could mainly be due to the hydrophilic sites of the composite membranes, which inhibited the hydrophobic interaction between the membrane surface and the foulant. The obtained results were also consistent with the contact angle measurements. This may also be supported by the FRR value declination after the further addition of MNPs (PVC-MNP 10%), which can be related to the decrease in the surface hydrophilicity after the addition of 10% of MNPs. Moreover, this would suggest the reversibility of SA fouling on the membrane surface is more likely, as a result of higher surface hydrophilicity and the presence of MNPs on the surface. Though it was reported that the fouling behavior is highly dependent on the layer hydrophilicity [32], the obtained results would suggest that hydrophilicity is not the only factor that can affect the antifouling. Other parameters, such as surface charge and surface roughness may also have an effect in controlling the antifouling characteristics of the membranes as reported by Vatanpour et al., where a similar opposite behavior was observed [23]. In addition, the porosity and pore size of the composite membrane, which also increased with the MNPs addition, may have an effect on the antifouling observed performance.

5. Conclusions

The presence of MNPs was found to result in an apparent enhancement of the PVC membrane performance. The pure water flux results demonstrated an improvement in the flux in tandem with an increase in the MNPs content. The composite membranes reached around 1310 L/m²h and rose up to around 55%, compared to the pure PVC. In particular, with regards to solute rejection efficiency, the composite membranes with 6% MNPs were found to display an optimum performance up to 93%, 94%, 88%, and 83% for NaCl, Na_2SO_4, $MgSO_4$, and LiCl, respectively. In addition to the enhanced water flux and solute rejection, enhanced antifouling properties and thermal stability were also observed.

Acknowledgments

The authors extend their appreciation to the Deanship of Scientific Research at King Khalid University for funding this work through the General Research Project under grant number (G.R.P-18-39 /2018)".

Symbols

ε	—	Membrane porosity
W_w	—	Weight for wet membrane
W_d	—	Weight for dry membrane
ρ_w	—	Density of water
r	—	Radius of membrane
l	—	Thickness of membrane
a	—	Mean pore diameter
μ	—	Viscosity of water
Q_w	—	Pure water flux
A	—	Filtration area
ΔP	—	Transmembrane pressure
V	—	Volume of permeate
t	—	Time interval
$SR\%$	—	Solute rejection percentage
C_f	—	Concentration of the feed
C_p	—	Concentration of the permeate
$FRR\%$	—	Flux recovery ratio
J_w	—	Pure water flux
J_{w1}	—	Pure water flux before fouling
J_{w2}	—	Pure water flux after fouling
D_c	—	Crystallite size
β	—	Full width at half maximum

References

[1] Y. Peng, Y. Sui, Compatibility research on PVC/PVB blended membranes, Desalination, 196 (2006) 13–21.

[2] J. Xu, Z.-L. Xu, Poly(vinyl chloride) (PVC) hollow fiber ultrafiltration membranes prepared from PVC/additives/solvent, J. Membr. Sci., 208 (2002) 203–212.

[3] E. Demirel, B. Zhang, M. Papakyriakou, S. Xia, Y. Chen, Fe_2O_3 nanocomposite PVC membrane with enhanced properties and separation performance, J. Membr. Sci., 529 (2017) 170–184.

[4] H. Wu, T. Li, B. Liu, C. Chen, S. Wang, J.C. Crittenden, Blended PVC/PVC-g-PEGMA ultrafiltration membranes with enhanced performance and antifouling properties, Appl. Surf. Sci., 455 (2018) 987–996.

[5] B. Liu, C. Chen, W. Zhang, J. Crittenden, Y. Chen, Low-cost antifouling PVC ultrafiltration membrane fabrication with Pluronic F 127: Effect of additives on properties and performance, Desalination, 307 (2012) 26–33.

[6] Z. Zhou, S. Rajabzadeh, A. Rajjak Shaikh, Y. Kakihana, T. Ishigami, R. Sano, H. Matsuyama, Preparation and characterization of antifouling poly(vinyl chloride-co-poly(ethylene glycol)methyl ether methacrylate) membranes, J. Membr. Sci., 498 (2016) 414–422.

[7] C. Güell, R.H. Davis, Membrane fouling during microfiltration of protein mixtures, J. Membr. Sci., 119 (1996) 269–284.

[8] A. Akthakul, R.F. Salinaro, A.M. Mayes, Antifouling polymer membranes with subnanometer size selectivity, Macromolecules, 37 (2004) 7663–7668.

[9] P. Wang, K.L. Tan, E.T. Kang, K.G. Neoh, Antifouling poly(vinylidene fluoride) microporous membranes prepared via plasma-induced surface grafting of poly(ethylene glycol), J. Adhes. Sci. Technol., 16 (2002) 111–127.

[10] F. Liu, C.H. Du, B.K. Zhu, Y.Y. Xu, Surface immobilization of polymer brushes onto porous poly(vinylidene fluoride) membrane by electron beam to improve the hydrophilicity and fouling resistance, Polymer, 48 (2007) 2910–2918.

[11] S.J. Oh, N. Kim, Y.T. Lee, Preparation and characterization of PVDF/TiO_2 organic–inorganic composite membranes for fouling resistance improvement, J. Membr. Sci., 345 (2009) 13–20.

[12] J.-F. Li, Z.-L. Xu, H. Yang, L.-Y. Yu, M. Liu, Effect of TiO_2 nanoparticles on the surface morphology and performance of microporous PES membrane, Appl. Surf. Sci., 255 (2009) 4725–4732.

[13] G. Wu, S. Gan, L. Cui, Y. Xu, Preparation and characterization of PES/TiO_2 composite membranes, Appl. Surf. Sci., 254 (2008) 7080–7086.

[14] V. Vatanpour, S.S. Madaeni, A.R. Khataee, E. Salehi, S. Zinadini, H.A. Monfared, TiO_2 embedded mixed matrix PES nanocomposite membranes: Influence of different sizes and types of nanoparticles on antifouling and performance, Desalination, 292 (2012) 19–29.

[15] X. Cao, J. Ma, X. Shi, Z. Ren, Effect of TiO_2 nanoparticle size on the performance of PVDF membrane, Appl. Surf. Sci., 253 (2006) 2003–2010.

[16] L. Shen, X. Bian, X. Lu, L. Shi, Z. Liu, L. Chen, Z. Hou, K. Fan, Preparation and characterization of ZnO/polyethersulfone (PES) hybrid membranes, Desalination, 293 (2012) 21–29.

[17] H. Rabiee, V. Vatanpour, M.H.D.A. Farahani, H. Zarrabi, Improvement in flux and antifouling properties of PVC ultrafiltration membranes by incorporation of zinc oxide (ZnO) nanoparticles, Sep. Purif. Technol., 156 (2015) 299–310.

[18] N. Maximous, G. Nakhla, W. Wan, K. Wong, Preparation, characterization and performance of Al_2O_3/PES membrane for wastewater filtration, J. Membr. Sci., 341 (2009) 67–75.

[19] X. Liu, Y. Peng, S. Ji, A new method to prepare organic-inorganic hybrid membranes, Desalination, 221 (2008) 376–382.

[20] J.-n. Shen, H.-m. Ruan, L.-g. Wu, C.-j. Gao, Preparation and characterization of PES–SiO_2 organic–inorganic composite ultrafiltration membrane for raw water pretreatment, Chem. Eng. J., 168 (2011) 1272–1278.

[21] J. Zhang, Z. Xu, M. Shan, B. Zhou, Y. Li, B. Li, J. Niu, X. Qian, Synergetic effects of oxidized carbon nanotubes and graphene oxide on fouling control and anti-fouling mechanism of polyvinylidene fluoride ultrafiltration membranes, J. Membr. Sci., 448 (2013) 81–92.

[22] V. Vatanpour, S.S. Madaeni, R. Moradian, S. Zinadini, B. Astinchap, Novel antibifouling nanofiltration polyethersulfone membrane fabricated from embedding TiO_2 coated multiwalled carbon nanotubes, Sep. Purif. Technol., 90 (2012) 69–82.

[23] V. Vatanpour, M. Esmaeili, M.H.D.A. Farahani, Fouling reduction and retention increment of polyethersulfone nanofiltration membranes embedded by amine-functionalized multi-walled carbon nanotubes, J. Membr. Sci., 466 (2014) 70–81.

[24] T.A. Agbaje, S. Al-Gharabli, M.O. Mavukkandy, J. Kujawa, H.A. Arafat, PVDF/magnetite blend membranes for enhanced flux and salt rejection in membrane distillation, Desalination, 436 (2018) 69–80.

[25] M.R. Mehrnia, M. Homayoonfal, Fouling mitigation behavior of magnetic responsive nanocomposite membranes in a magnetic membrane bioreactor, J. Membr. Sci., 520 (2016) 881–894.

[26] P. Daraei, S.S. Madaeni, N. Ghaemi, M.A. Khadivi, B. Astinchap, R. Moradian, Fouling resistant mixed matrix polyethersulfone membranes blended with magnetic nanoparticles: Study of magnetic field induced casting, Sep. Purif. Technol., 109 (2013) 111–121.

[27] B. Deng, M. Yu, X. Yang, B. Zhang, L. Li, L. Xie, J. Li, X. Lu, Antifouling microfiltration membranes prepared from acrylic acid or methacrylic acid grafted poly(vinylidene fluoride) powder synthesized via pre-irradiation induced graft polymerization, J. Membr. Sci., 350 (2010) 252–258.

[28] H.P. Klug, L.E. Alexander, X-ray diffraction procedures: for polycrystalline and amorphous materials, 2nd ed., John Wiley & Sons, New York, 1974.

[29] A.K. Shukla, J. Alam, M. Alhoshan, L.A. Dass, M.R. Muthumareeswaran, Development of a nanocomposite ultrafiltration membrane based on polyphenylsulfone blended with graphene oxide, Sci. Rep., 7 (2017) 41976.

[30] S. Qiu, L. Wu, X. Pan, L. Zhang, H. Chen, C. Gao, Preparation and properties of functionalized carbon nanotube/PSF blend ultrafiltration membranes, J. Membr. Sci., 342 (2009) 165–172.

[31] H. Wu, B. Tang, P. Wu, Novel ultrafiltration membranes prepared from a multi-walled carbon nanotubes/polymer composite, J. Membr. Sci., 362 (2010) 374–383.

[32] J. Lv, G. Zhang, H. Zhang, F. Yang, Exploration of permeability and antifouling performance on modified cellulose acetate ultrafiltration membrane with cellulose nanocrystals, Carbohydr. Polym., 174 (2017) 190–199.